CEAS Space Journal (2023) 15:827–844
https://doi.org/10.1007/s12567-023-00502-2

ORIGINAL PAPER

Combustion characteristics of a supersonic combustor model for a JAXA flight experiment

Masahiro Takahashi[1] · **Kan Kobayashi**[1] · **Sadatake Tomioka**[1]

Received: 30 November 2022 / Revised: 30 April 2023 / Accepted: 1 May 2023 / Published online: 15 May 2023

Abstract
JAXA is conducting a flight-ground test comparison program to clarify the "facility effect" on hypersonic aerodynamics and combustion phenomena and to develop a CFD tool for predicting flight data from ground test data. The aim is a flight experiment to obtain data on aerodynamic heating and supersonic combustion under actual flight conditions and to validate the CFD tool using flight data and the corresponding ground test data. This study aimed at determining a flow-path geometry and a fuel injector configuration for a supersonic combustor suitable for clarifying the influence of the different test flow compositions between flight and ground test conditions on combustion. The candidate configurations proposed by the CFD study were evaluated by direct-connect combustion tests using ethylene fuel. The results showed that a combustor flow was symmetric when the fuel equivalence ratio was low and asymmetric when the equivalence ratio and the pressure in the combustor were high. Because an asymmetric flow is unsuitable for validating CFD based on steady RANS, the total equivalence ratio was limited to 0.44. The combustor model uses two-stage fuel injectors and cavity flame holders to combust ethylene fuel. The depth of the cavity flame holder had little influence on combustion. However, the number of injection holes for the injector located downstream of the cavity affected the combustor pressure. The combustor flow-path design was finalized based on the combustion test results. In addition, an ethylene fuel ignition method using pilot hydrogen injection, adopted for the flight experiment, was also demonstrated successfully.

Keywords Supersonic combustion · Ground testing · Flight experiment · Hydrocarbon fuel · CFD

1 Introduction

Research and development of hypersonic air-breathing propulsion systems, such as the scramjet, have been actively conducted worldwide. Both ground tests and CFD play essential roles in their development. Making the best use of these is expected to reduce the number of necessary flight tests and development costs.

To apply the combustion test data to an engine design, however, it is necessary to consider the influence of the flow characteristics on this data, which the ground test facility produces (i.e., the "facility effect"). For example, it is necessary to heat the airflow to reproduce the high-speed airflow in the wind tunnel corresponding to the scramjet operating conditions. JAXA has built a large blowdown wind tunnel for high-speed air-breathing engine testing at the Kakuda Space Center, also known as the Ramjet Engine Test Facility (RJTF) [1]. The RJTF can reproduce flow conditions for hypersonic air-breathing engine tests that correspond to flight at Mach 4, 6, and 8. The facility can test an engine model up to 3 m long. The RJTF has two types of airflow-heating devices: a storage air heater (SAH) and a vitiation air heater (VAH). The SAH heats the airflow by heat exchange with hot bricks, while the VAH raises the total temperature of the airflow by adding hydrogen and oxygen to the airflow and burning them. The oxygen concentration in the VAH test flow is kept at 21 mol%, but water vapor is introduced into the test flow. The unique capability of the RJTF is that both the SAH and VAH can reproduce the test flow conditions corresponding to Mach 6 flight. Past work has shown different combustion test results for various airflow-heating

✉ Masahiro Takahashi
takahashi.masahiro@jaxa.jp

Kan Kobayashi
kobayashi.kan@jaxa.jp

Sadatake Tomioka
tomioka.sadatake@jaxa.jp

[1] Japan Aerospace Exploration Agency (JAXA), Kakuda, Miyagi 981-1525, Japan

methods [2]. This is believed to be caused by the influence on combustion of a difference in the flow enthalpy and water vapor in the VAH test flow. The latter is known as the "vitiation effect." Since test flow conditions beyond Mach 6 flight cannot be reproduced without the VAH, such phenomena must be clarified.

The "vitiation effect" in ground testing of hypersonic air-breathing engines has been the subject of much research since the late 1960s. Pellet et al. [3] conducted a detailed review of the effects of major and minor species on ignition and flame holding in scramjets, drawing on over 100 references. In the last decade, an electrically heated, clean-air, supersonic wind tunnel at the University of Virginia has been used to report the results of scramjet combustor tests using pure air and a mixture of air, water vapor, and CO2, simulating the test flow in a combustion-heated wind tunnel. Rockwell et al. [4] tested a hydrogen-fueled combustor with a ramp injector at the test flow total temperature of 1200 K, equivalent to flight Mach 5 conditions. They showed that the test gas of air mixed with water vapor and CO2 resulted in lower combustion pressure and shorter length of the shock train in the subsonic combustion mode case, and a higher equivalence ratio condition, at which the transition between subsonic and supersonic combustion modes occurred than pure air. Tatman et al. [5] also reported the effect of test flow composition on the flameout limit of an ethylene-fueled scramjet model with a cavity flame holder using the same facility and test flow conditions. Several flight tests of hydrocarbon-fueled scramjets have been conducted, but test results are rarely published in the open literature.

Therefore, JAXA has started a five-year research program to understand the influence of the flow turbulence and the difference in the test flow composition between the flight and ground test conditions on aerodynamic heating and combustion. We propose to solve this issue by predicting the combustion characteristics and aerodynamic heating under actual flight conditions using a CFD tool, whose model parameters are tuned so that the tool can reproduce the ground test results. To establish this methodology, we plan to conduct both a flight experiment to obtain the supersonic combustion and aerodynamic heating data from actual flight and post-flight-ground tests. The test flow conditions would be adjusted to match the airflow conditions of the flight test to produce sets of flight test and ground test data under similar airflow conditions. The model parameters of the CFD tool will be tuned so that the ground test data can be reproduced. Then this tuned tool will be applied to predict the combustor flow under the flight test conditions to verify whether the flight test results can be reproduced with this methodology [6]. Steady RANS was adopted as the CFD prediction tool for our research program. The primary reasons are the following. First, Nagata et al. investigated the influence of free-stream turbulence on the supersonic transverse jet mixing process numerically by performing LES. They showed no clear difference between the cases with and without free-stream turbulence, whose intensity was up to 2.2% of mean free-stream velocity, observed on the mean and instantaneous flow fields [7]. Therefore, we focused on predicting the influence of water vapor in the facility test flow on combustion rather than mainstream turbulence, which most likely requires LES [8]. Second, we aim to develop a practical CFD tool that can be used for the parametric design study of scramjet engines. It is still challenging to apply LES or Hybrid LES/RANS to the practical design of supersonic combustors because of the enormous computational cost.

Figure 1 shows a schematic of the JAXA RD1 flight experiment vehicle (FEV) for supersonic combustion. It is 1.75 m long. The FEV will be launched by an S-520 rocket. The FEV has an axisymmetric shape, which fits into the nose cone of the launcher. After acceleration by the launcher, the FEV separates and continues to fly along a ballistic trajectory. The supersonic combustion experiment will be conducted in the descent phase when the FEV is re-accelerated to reach Mach 6. The combustor model is vertically symmetrical and is mounted along the FEV central axis. Considering the inlet start capability at a low flight Mach number before the combustion experiment starts, an alligator-type inlet is adopted. In addition, the inlet is a mixed-compression-ramp type to minimize the length and tip height to fit in the nose cone and consists of external and internal compression-ramp sections. Airflow is first compressed in the vertical direction by the external ramps on the top and bottom walls and then in the horizontal direction by the internal ramps on both side wall tips. The internal flow path downstream of the internal-inlet section consists of an isolator, a combustor, and a downstream extension duct. The isolator is a rectangular duct 38.1 mm high, 50.8 mm wide, and 300 mm long. The isolator prevents a flow disturbance caused by high

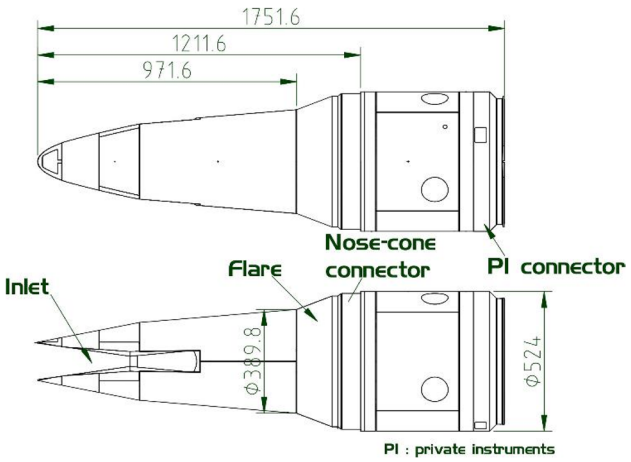

Fig. 1 Schematic of JAXA RD1 flight experiment vehicle for supersonic combustion

pressure in the combustor from propagating back into the inlet and causing an inlet unstart. The combustor flow path is represented two-dimensionally and diverges symmetrically vertically. The fuel is gaseous ethylene, ignited by the self-ignition of gaseous hydrogen as a pilot fuel instead of using a torch ignitor or a spark plug. This reduces the electric power consumption of the FEV and mitigates high voltage leakage risk. The wall pressure distribution in the combustor model is measured as supersonic combustion data. In addition, the aerodynamic heating of the FEV surface and the turbulence intensity of the airflow captured by the inlet of the combustor model will also be measured in flight.

This study focused on the vitiation effect, namely the influence of the difference in test-flow compositions on combustion. The internal flow-path design of the combustor model is one of the most critical issues in designing the RD1 FEV. The first steps of the flow-path design, 1D analysis, and 3D CFD design have been performed for the supersonic combustor flow to establish the flow-path design guidelines for the model [9, 10]. The primary requirements for the flow-path design were the following: First, a sizable difference in the wall pressure distribution is obtained due to the difference in the composition of the combustor's incoming flow between the flight and facility conditions. Second, supersonic-combustion mode operation is achieved because of the relatively simple flow structure in the combustor, a higher sensitivity to the difference in the flow composition due to lower pressure and lower temperature in the combustor, and less risk of transition to a catastrophic inlet unstart during the flight test than in the subsonic-combustion mode. The CFD study showed that increasing the fuel equivalence ratio while preventing the transition to the subsonic-combustion mode is necessary to satisfy the first design requirement. The target value determined by the CFD study was a total equivalence ratio of 0.5 [9, 10]. Past studies on wall injection into a supersonic crossflow reported that the mixing process changes significantly depending on whether pseudo-shock waves are formed [11]. It was also reported that the shape of the fuel-injector hole affects the mixing efficiency when the injector is in an attached flow region, while the mixing efficiency becomes less sensitive to the hole shape when the injector is in a separated flow region [12]. The presence of pseudo-shock waves and large-scale separated flows due to the subsonic-combustion mode operation complicates the flowfield, making CFD prediction difficult. In addition, detecting a change in the combustion characteristics due to a difference in the composition of the incoming flow would also be problematic. Therefore, the establishment of a supersonic combustion mode operation is essential. Note that this research targets the combustor operation conditions, in which the velocity of the test flow is high and cannot be reproduced without using the VAH. However, with a high-temperature flow, the pressure rise due to combustion tends to be small, so the combustor operation is likely to be in the supersonic combustion mode. Thus, aiming to establish the supersonic combustion mode is consistent with the high-velocity airflow conditions sought by the current research.

The purpose of the present study is to conduct combustion tests of the supersonic combustor model for our flight experiment with the candidate configurations proposed by the CFD study and to determine the combustor configuration and its operating conditions so that a sizable difference would appear between the pressure data of the flight test and those of the ground test due to the difference in the airflow composition. Soon after we started the combustion test campaign, we realized that a symmetric combustor flow could be maintained when the total equivalence ratio of the ethylene fuel was low. However, the combustor flow became vertically asymmetric as the fuel equivalence ratio increased and the pressure in the combustor became high, although the supersonic combustion mode was still maintained. The CFD for the design study assumed that the combustor flow was vertically and laterally symmetric. Thus, the CFD could never predict an asymmetric combustor flow. As mentioned, the current project's target was to develop a practical CFD tool based on steady RANS. Therefore, test data taken from such an asymmetric combustor flow are unsuitable for CFD validation because it would be considerably more difficult for the CFD to simulate than a symmetric flow. By considering the new findings, the second requirement for the combustor flow-path design was modified so that a symmetric combustor flow in the supersonic combustion mode would be established. The first design requirement remained the same. The influence of the shapes of the cavity flame holder and fuel-injector holes and the fuel supply conditions on the combustion characteristics were clarified, and both the combustor flow-path design and the fuel supply condition were determined suitable for the RD1 flight experiment. In addition, the ignition method for ethylene fuel using pilot hydrogen injection was adopted for the RD1 flight experiment. Since the current ignition method is not commonly used, it was also demonstrated in the combustion tests.

2 Combustion test

2.1 Combustor model

This study investigated the influence on combustion of the difference between the test flow compositions under the flight and ground test conditions. The requirements for the flow-path design were the following: First, there are sizable differences in the wall pressure profile between the ground test and flight test because of the composition difference in incoming combustor flows. Second, the symmetric combustor flow in supersonic-combustion mode operation is

established under flight and ground test conditions. The CFD study showed that increasing the fuel equivalence ratio while maintaining supersonic combustion is necessary [9]. Since it was reported that a combustor adopted for the HIFiRE Flight 2 experiment achieved the supersonic-combustion mode operation with a total fuel equivalence ratio of unity and combustion efficiency of 0.7 or higher at flight Mach 8 [13], its flow-path configuration was used as a reference for the baseline design. When we made the design study, the flight experiment's representative Mach number and dynamic pressure were set to 6.1 and 62.5 kPa, respectively. These values are different from those for the HIFiRE 2. Therefore, modification of the flow-path has been studied by CFD [9, 10].

Figure 2 shows an example of the supersonic combustor flow-path configuration, which uses a 2D diverging-area duct combustor. The combustor flow path was vertically symmetrical. The top and bottom walls have a half-diverging angle of 1.3°, and the combustor entrance was 38.1 mm high and 50.8 mm wide. Two-stage fuel injection was chosen. The fuel supplied by the upstream injector (i.e., Injector 1) burned well with the assistance of the cavity flame holder to raise the cavity pressure, expected to increase the influence of the test flow total enthalpy and the water vapor in the test flow on the cavity pressure. The combustion of the Injector 1 fuel was also expected to supply radicals that promote the ignition and flame holding of ethylene from the downstream injector (i.e., Injector 2). The pressure rise caused by the Injector 2 fuel combustion was assumed to be a reliable indicator of the water vapor's influence on ignition delays and combustion heat release in the expanding flow. As in the injector configuration of the HIFiRE 2 combustor, which also used two-stage injection, the angles of Injectors 1 and 2 were 15° and 90° from the combustor wall, respectively. A large cavity flame holder was mounted between the two injectors on each wall. The combustion test provided information on the influence of the following parameters on the combustion characteristics:

(1) The fuel equivalence ratio of Injectors 1 and 2;
(2) The depth of the cavity flame holder;
(3) The diameter, the number, and the lateral spacing of the injection holes for Injector 1; and
(4) The diameter, the number, and the lateral spacing of the injection holes for Injector 2.

The value of each parameter is summarized in Table 1. Three values of the total fuel equivalence ratio were compared: 0.38, 0.44, and 0.54. The influence of the split ratios of the ethylene fuel supplied by Injectors 1 and 2 on combustion was also investigated for the total equivalence ratios of 0.44 and 0.54. For example, the same amount of ethylene was supplied from Injectors 1 and 2 in cases 2 and 4, although the total equivalence ratios differed. However, less ethylene was supplied from Injector 1 than Injector 2 for the other cases to lower the pressure in the cavity and prevent transitioning to asymmetric combustor flow or to the subsonic-combustion mode. In the cavity depth comparison, the aperture length (defined as the length from the upstream cavity edge to the cavity aft-ramp end) was fixed at 159 mm so that air would be entrained into the cavity at approximately the same mass flow rate for all three cavities through the shear layer between the main airflow and the cavity recirculating flow. The amount of flow expansion due to the sudden expansion of the flow-path cross-section in the cavity and the residence time of the fuel–air mixture in the cavity differs with cavity depth. For Injectors 1 and 2, the diameter of the injection hole is the scale factor for fuel penetration height; the number of holes is likely to change flow blockage due to the difference in the distribution of combusting fuel flows. The lateral spacing between injector holes was also thought to affect the lateral distribution of the fuel.

The following parameters were fixed in this study. In the combustor geometry, the half expansion angle of the top and bottom walls of the combustor was 1.3°. The diverging-area combustor was 38.1 mm high and 50.8 mm wide at

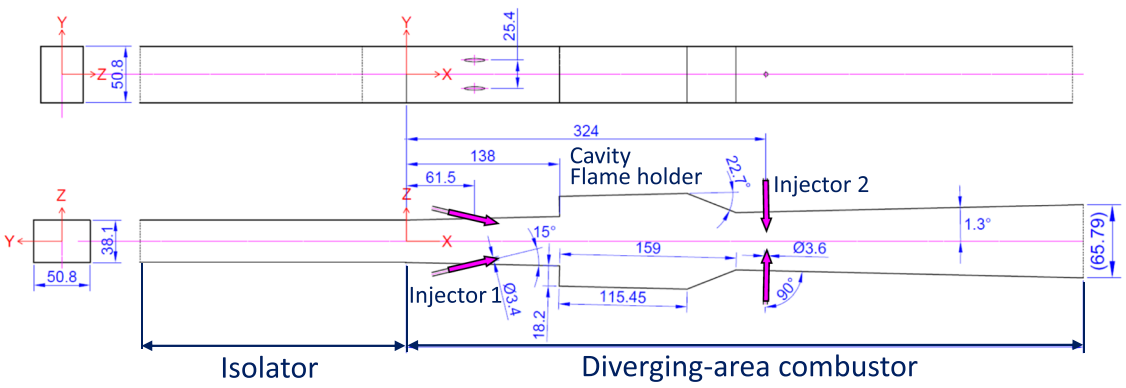

Fig. 2 Example of combustor flow-path configuration

Table 1 Parameters for the combustion tests

Equivalence ratio	Case	Injector 1	Injector 2	Total equiv. ratio
	1	0.16	0.22	0.38
	2	0.22	0.22	0.44
	3	0.17	0.27	0.44
	4	0.27	0.27	0.54
	5	0.10	0.33	0.43
	6	0.20	0.33	0.53
Cavity depth	Type	Depth (mm)	Aperture length (mm)	Aft-ramp angle (°)
	α	25.7	159	22.7
	β	18.2		
	γ	12.85		
Injector 1	Type	Diameter (mm)	Number of holes	Spacing (mm)
	a	4.8	1	–
	b	3.4	2	25.4
	c	3.4	2	17
	d	2.4	2	17
Injector 2	Type	Diameter (mm)	Number of holes	Spacing (mm)
	A	3.6	2	25.4
	B	3.6	1	–
	C	2.5	2	17
	D	2.5	1	–

the entrance, and 610 mm long. The geometry of the cavity flame holder reflects an aperture length of 159 mm and an aft-ramp angle of 22.7°; the cavity flame holder was mounted 138 mm downstream from the entrance of the combustor. Injector 1 was mounted 61.5 mm downstream from the combustor entrance, and the injection angle was 15° relative to the combustor wall. Injector 2 was installed 324 mm downstream from the combustor entrance. Normal injection was used.

The combustor model consisted of four plates—a top wall, a bottom wall, and two side walls—and a flange attached at the upstream end. The combustor model was uncooled. All the plates were made from oxygen-free copper. The top and bottom plates were 43 mm thick, and the side plates were 30 mm thick. To shorten the manufacturing time because of the tight schedule, all these plates were bolted together to assemble the combustor, and a GRAFOIL® sheet (NeoGraf Solutions) 0.7 mm thick was inserted between all the contact surfaces of the plates for sealing. The injector and cavity flame holder blocks were also bolted to the top and bottom plates so that they could be replaced. Synthetic quartz glass, 300 mm wide, 70 mm high, and 25 mm thick, was mounted on one of the side walls to allow the flame inside the combustor to be observed.

2.2 Test facility

The combustion tests used a supersonic wind tunnel with the VAH in the JAXA Kakuda Space Center, the KWT. Mixing and burning hydrogen and oxygen in the high-pressure airflow raises the total temperature of the airflow, and the high-temperature, high-pressure airflow expands through the facility nozzle and becomes a high-speed airflow. Oxygen is added so that the oxygen concentration in the test flow after the combustion heating is maintained at 21%mol, the same as ambient air. The combustion test was conducted in a direct-connect configuration. The combustor model was connected to the facility nozzle exit via a 240 mm long constant-area duct isolator. The facility nozzle flow simulated the airflow compressed by the inlet of the RD1 FEV in flight. The inner walls of the VAH plenum chamber, the cross-sectional shape conversion duct, the nozzle, and the isolator duct were water-cooled. The mass flow rates of air, hydrogen, and oxygen supplied to the VAH were measured by orifice flowmeters of the facility gas supply system. Figure 3 shows the combustor model installed in the KWT. The combustor model was installed by rotating 90° around its center axis so that the side wall with the observation window was facing up. In Fig. 3, the walls facing to the right and left

Fig. 3 The combustor model installed in the KWT at JAXA Kakuda Space Center

were designated the top and bottom walls, on which the fuel injectors and the cavity flame holder were mounted.

The facility test flow conditions were set at a total pressure of 2 MPa and a total temperature of 1700 K. The details of the test flow conditions are summarized in Table 2. The Mach 3 facility nozzle supplied the high-speed airflow to the combustor model. It is a two-dimensional nozzle, the flow path of which converges and diverges in the height direction. The throat is 6.31 mm high, and the exit is 38.1 mm high. It is 50.8 mm wide. The nozzle was designed so that the core flow Mach number of the facility flow matched the cross-sectional average Mach number of the airflow after compression by the inlet of the RD1 FEV under the representative flight test conditions; those were flight Mach 6.1 and a dynamic pressure of 62.5 kPa.

2.3 Fuel supply system

Figure 4 shows the fuel supply system used in the combustion tests. The primary fuel was gaseous ethylene. To prevent ethylene condensation due to adiabatic expansion in the fuel supply lines, ethylene was warmed to 40 °C by putting the

Table 2 Test flow conditions

Total pressure, MPa	$1.994\times(1\pm0.61\%)$
Total temperature, K	$1692\times(1\pm1.1\%)$
Mole fraction in facility flow	
Oxygen	$0.2188\times(1\pm0.59\%)$
Water vapor	$0.2014\times(1\pm1.5\%)$
Total mass flow rate, kg/s	$0.6464\times(1\pm1.4\%)$
Component	
Air, kg/s	$0.5083\times(1\pm1.6\%)$
Oxygen, kg/s	$0.1283\times(1\pm0.78\%)$
Hydrogen, kg/s	$0.00974\times(1\pm1.5\%)$

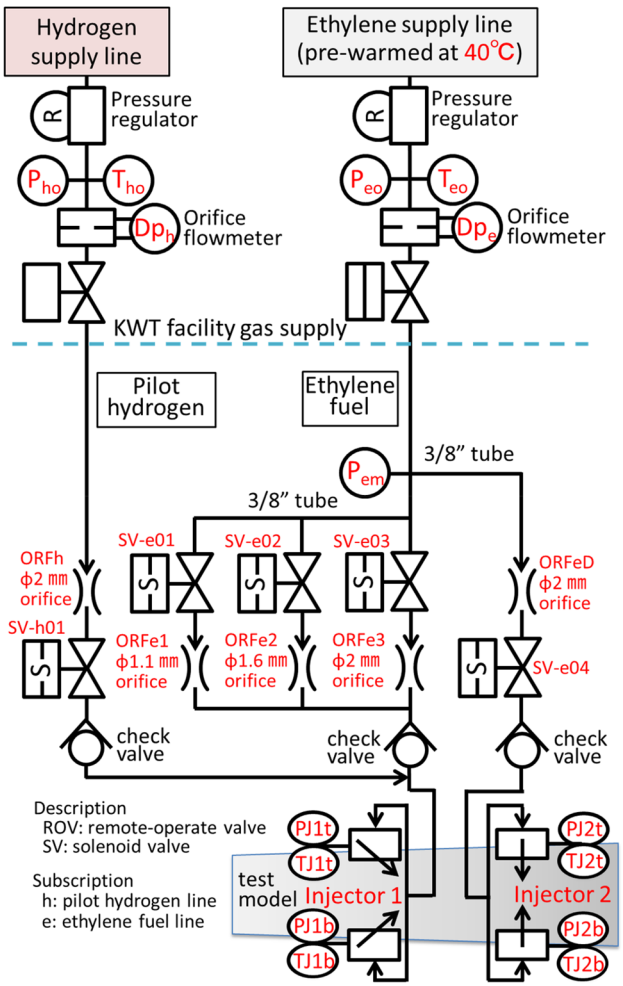

Fig. 4 Fuel supply system

ethylene cylinder in a hot water tub before being supplied to the combustor model. By inserting an orifice into the fuel supply pipe near the combustor model to choke the flow, the mass flow rate of the fuel supplied to the combustor model was determined. At the same time, the combustor model was acoustically isolated from the fuel supply system of the wind tunnel. The ethylene supply pipe branched into pipes to Injectors 1 and 2. The pipe to Injector1, in turn, branched into three pipes, each equipped with a solenoid valve and an orifice with different hole diameters (i.e., 1.1 mm, 1.6 mm, and 2 mm). In contrast, the pipe to Injector 2 did not branch and had only an orifice with a 2 mm-diameter hole. The split ratio of the ethylene mass flow rate supplied to Injectors 1 and 2 could be changed during a test by switching the pipe to Injector 1 with the solenoid valves. The total mass flow rate of ethylene fuel was determined by the combined resistance of the orifices attached to the pipes supplying to Injectors 1 and 2 and the ethylene supply pressure set by a regulator of the facility supply system. The total mass flow rate of ethylene fuel was measured by an orifice flowmeter of the facility

supply system. The fuel mass flow rate supplied to Injectors 1 and 2 was determined by multiplying the measured total mass flow rate by the split ratio calculated from the orifice hole diameter and its discharge coefficient. The largest hole of the orifices inserted into the ethylene supply pipe to Injectors 1 and 2 was 2 mm in diameter. The cross-sectional area at these orifice holes was the smallest in the ethylene supply system. Thus, the flow always choked at these orifices whenever ethylene was supplied at a suitable pressure.

2.4 Ignition method of ethylene fuel

In the RD1 flight experiment, the method for igniting ethylene fuel was pilot hydrogen injection. It is difficult to install a torch igniter or a spark plug on the RD1 FEV to reduce electric power requirements and mitigate high voltage leakage risk. Since the current ignition method is not commonly used, its feasibility was also examined in the combustion tests. Hydrogen is a highly reactive gas, so it easily self-ignites. The ignition method injects pilot hydrogen gas to achieve self-ignition and flame holding. Note that the pilot hydrogen was supplied only by Injector 1, which was upstream of the cavity flame holder, so the long residence time of hydrogen in the cavity ensured its self-ignition. Then, ethylene fuel started to flow and was ignited by the pilot hydrogen flame. Finally, the pilot hydrogen supply was stopped, and pure ethylene combustion started. At first, the ignition method was demonstrated by supplying the pilot hydrogen gas using the hydrogen gas supply system of the KWT steadily. After confirming that the method worked, it was used in the subsequent combustion tests. In addition, we also demonstrated the ignition method by supplying the pilot hydrogen gas from a 1 L run tank in a blowdown manner, assuming application to the actual RD1 FEV.

The pilot hydrogen supply system is also shown in Fig. 4 and is similar to the ethylene supply system. An orifice with a 2 mm-diameter hole in the supply line determined the hydrogen mass flow rate by choking the flow. The supply pressure was 2.2 MPa, resulting in a hydrogen equivalence ratio of 0.21.

2.5 Measurements

In the combustion test, wall pressure was measured by 42 and 39 ports mounted along the center lines of the top and bottom walls, with 7 ports on the side wall with the observation window and 38 ports on the other side wall. There were 126 wall pressure measurement ports in total. A PSI (Measurement Specialties Inc., System 8400) was used to simultaneously measure the wall pressure at multiple points. One 64-channel gauge-pressure scanner head with a 410 kPa range and one with a 790 kPa range were connected to the System 8400. The sampling frequency was 20 Hz for each channel. In addition, the ethylene flame in the combustor was recorded with a commercial video camera (Sony HDR-CX670).

3 Results and discussion

3.1 Combustion test overview

A preset automatic sequence controlled the wind tunnel operation and the fuel supply during a combustion test, except for the supply of the facility cooling water and the main airflow, which were controlled manually by the facility operator. An example of the combustion test sequence is shown in Fig. 5. The origin of time t is the time when the automatic sequence starts operating. In a combustion test, the data acquisition, the facility cooling water supply, and the room-temperature main airflow supply were manually started. The automatic sequence was manually started when the airflow supply became steady. At $t=5$ s, the VAH started supplying a nozzle flow with a total temperature of 1100 K by adding only a small amount of hydrogen to the airflow, igniting it with a spark plug, and burning it. The 1100 K nozzle flow gradually pre-heated the observation window

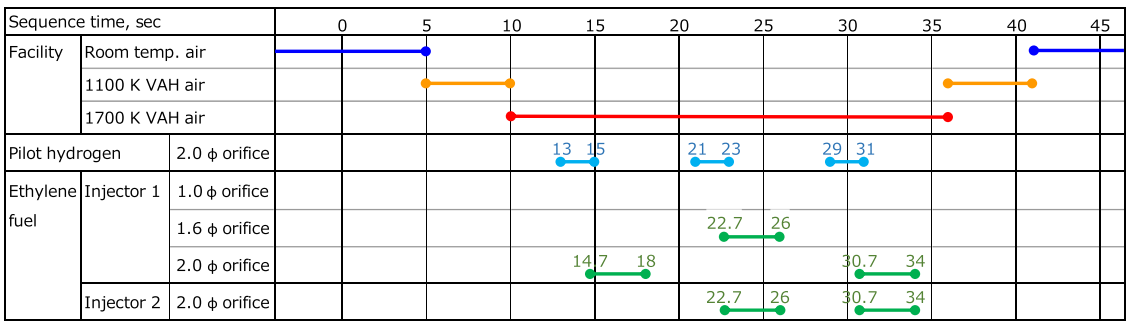

Fig. 5 Example of combustion test sequence

glass to prevent cracking due to thermal shock. At $t = 10$ s, the facility was switched to supply the test flow with a total temperature of 1700 K by adding hydrogen and oxygen to the airflow. Adding oxygen maintained the oxygen concentration of 21 mol% in the VAH test flow. Every time the VAH operation was switched, the spark plug for the VAH was energized for 1.5 s to ignite the additional fuel supplied to the VAH.

In the case shown in Fig. 5, a pilot hydrogen and ethylene fuel supply check was performed three times within a single combustion test with a non-fueling interval of 3 s. Each time, pilot hydrogen was supplied for 2 s only from Injector 1, and it self-ignited instantaneously. Then ethylene supply started 1.7 s after the hydrogen supply started. It was ignited by the hydrogen flame within 0.3 s when hydrogen and ethylene were supplied simultaneously. The mass flow rate supplied from Injector 1 could be changed during a single test by switching the flow path to an orifice with a different diameter hole. In contrast, the Injector 2 mass flow rate was fixed because the supply line had no alternative flow path. It could be changed only by changing the supply pressure. The 1700 K test flow supply continued until $t = 36$ s when the facility was switched back to supply the 1100 K total temperature flow to gradually cool the window for 5 s. At $t = 41$ s, the hydrogen supply to the VAH was stopped, and then only room-temperature air was supplied to cool the facility and the combustor model. The facility's cooling water also continued to cool down the facility.

Time histories of the wall pressure in the combustor model and the total pressure of the nozzle flow measured in the VAH plenum chamber are shown in Fig. 6. Time histories of the combustor wall temperature and the fuel manifold pressure for Injectors 1 and 2 are shown in Fig. 7. The data were recorded during a combustion test using the sequence shown in Fig. 5. The fuel equivalence ratios of ethylene fuel

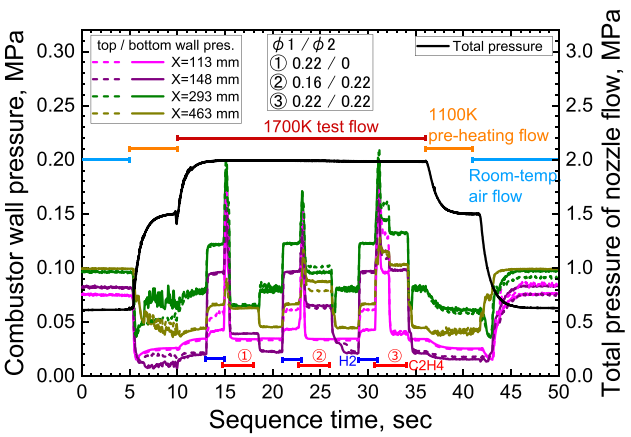

Fig. 6 Time history of combustor wall pressure and total pressure of test flow

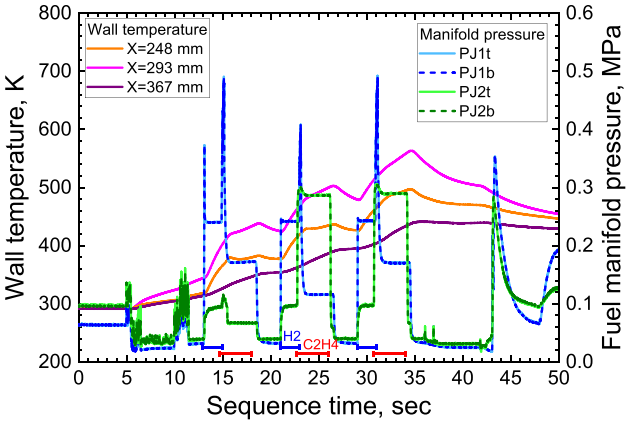

Fig. 7 Time history of combustor wall temperature and fuel manifold pressure

supplied to Injectors 1 and 2 in the first to the third sets were 0.22/0, 0.16/0.22 and 0.22/0.22, respectively. The blue and red bars at the bottom of each figure indicate when the pilot hydrogen and ethylene fuel were supplied, respectively. The bars above the time history in Fig. 6 indicate the facility nozzle flow status.

As shown in Fig. 6, the total pressure of the nozzle flow was a low 0.06 MPa when only room-temperature air was supplied. The pressure in the combustor model was 0.07 to 0.1 MPa, which was close to the atmospheric pressure, and the flow in the combustor model was likely to be accompanied by large-scale separation.

At $t = 5$ s, the VAH started to supply the pre-heated flow with an 1100 K total temperature, and the total pressure started to rise. The pressures in the combustor model all dropped except for $X = 293$ mm. The pressure port at $X = 293$ mm was located on the cavity aft-ramp. When fuel was not supplied or not burning, the pressure at $X = 293$ mm was high because the shear flow between the main airflow and the recirculating flow in the cavity flame holder strongly impinged on the cavity aft-ramp and produced a shock wave.

At $t = 10$ s, the VAH was switched to supply the test flow with a 1700 K total temperature, and the total pressure started to rise again and reached the target value of 2 MPa at $t = 13$ s so that the test flow was established. The total pressure was maintained almost constant at 2 MPa for 23 s. The first pilot hydrogen injection started when the test flow was established at $t = 13$ s. The wall pressure measured at the four points on the combustor model's top and bottom walls increased simultaneously and instantaneously, indicating that the pilot hydrogen self-ignited instantaneously. When pilot hydrogen and ethylene fuel were supplied simultaneously, the pressure at all four points increased rapidly. After that, when the hydrogen supply was stopped, and only the ethylene fuel was supplied, the pressure at all four points dropped and settled to a constant value at each point.

Then, when the ethylene supply was stopped at $t = 18$ s, the pressure dropped at the positions except for $X = 293$ mm, where the pressure rose due to the impinging shear flow, as described earlier. Injection of pilot hydrogen and ethylene fuel was performed three times, with 3 s without fueling. The pressure in the combustor model changed immediately following the change in the fuel supply conditions, and it remained almost constant while only ethylene fuel was supplied. However, an exception was noted during the ethylene fuel supply in the third set. The pressure in the combustor model continued to change until $t = 32.3$ s; after that, the pressures at all four points dropped simultaneously and settled to a constant value at each point. While pilot hydrogen and ethylene fuel were injected simultaneously at $t = 31$ s, the pressure in the combustor model became very high. A significant difference in the pressure distribution between the top and bottom walls was observed, making the combustor flow remarkably asymmetric. It is believed that the transition from significantly asymmetric to symmetric flow took time to cause the response delay in settling down the combustor flow.

At $t = 36$ s, the VAH was switched back to the pre-heating flow mode, and the total pressure started to drop. At $t = 42$ s, the VAH was turned off, and only room-temperature air was supplied to the combustor model. The total pressure dropped to 0.06 MPa, and the pressure in the combustor increased from 0.07 to 0.1 MPa. These data were quite similar to the initial flow condition when the automatic sequence control of the combustion test started.

The time histories of the fuel manifold pressure on the top and bottom walls are shown in Fig. 7. The data name shown in the legend corresponds to the pressure measurement point name in Fig. 4. First, the pressure histories of the fuel manifold on the top and bottom walls agreed well for each injector, suggesting that fuel supply from the top and bottom walls seemed to be even. Second, the fuel manifold pressures closely followed the pilot hydrogen and ethylene fuel supply conditions. The wall temperatures of the combustor model, also shown in Fig. 7, began to rise at the start of the hot airflow produced by the VAH. The wall temperature rose quickly during the pilot hydrogen injection but slowed when the fuel switched from hydrogen to ethylene. The wall temperature began to decrease when the fuel supply was stopped. In this combustion test, when the ethylene fuel supply in the third set was stopped, the wall temperature at the cavity aft-ramp rose to 560 K.

Note that the high-frequency fluctuations observed in the time histories of the fuel manifold pressure from $t = 5$ s to $t = 6.5$ s and those from $t = 10$ s to $t = 11.5$ s were due to electric noise caused by a spark plug used to ignite hydrogen supplied to the VAH. In addition, a sudden rise of the fuel manifold pressure at $t = 43$ s, when the combustion test had already finished, was due to discharging of the remaining fuel in the fuel supply lines by opening the solenoid valves from SV-e01 to SV-e04 and SV-h01 shown in Fig. 4. The other rise of the fuel manifold pressure at $t = 48$ s was caused by purging the fuel supply lines with nitrogen gas.

3.2 Combustor flow structure

An example of the CFD result for the current combustor flow is shown in Fig. 8 to describe the basic structure of the combustor flow. As for the numerical method, JAXA in-house code LS-FLOW [14] was used for the 3D RANS simulation with a SLAU2 scheme [15] for convection-term discretization, SST-V model of Menter [16] for turbulence modeling, and a 23-species skeletal reaction mechanism [17] for ethylene–air combustion chemistry. The turbulent Schmidt and Prandtl numbers were assumed to be 0.3 and 0.89, respectively. The cavity was type β. The configurations of Injectors 1 and 2 were types b and B, respectively. The fuel equivalence ratio set was case 2: 0.22 and 0.22 for Injectors 1 and 2. In each figure, the main airflow moves from left to right.

Figure 8a shows streamline traces in the half-space in the lateral direction. The line color indicates the local static temperature. The Mach number contour on the central symmetric plain in the lateral direction is shown in Fig. 8b, in which a black line represents a sonic line.

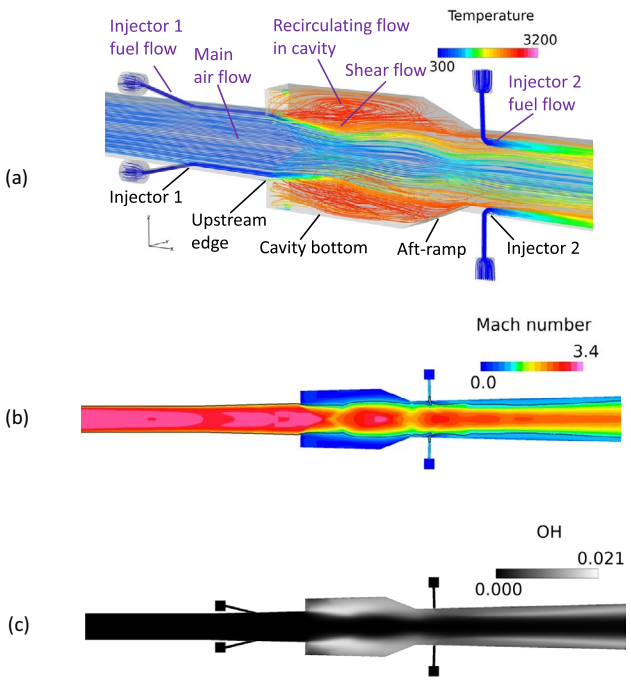

Fig. 8 Schematic of combustor flow structure predicted by CFD. **a** Streamline traces in half-space in the lateral direction; color shows static temperature. **b** Mach number contour on central symmetric plain in the lateral direction; a black line shows a sonic line. **c** Contour of OH radical mass fraction averaged in the lateral direction

The main airflow moved around the center of the combustor cross-section and remained supersonic throughout the combustor. The recirculating flow was formed in the cavity flame holder, where the temperature was high, and the Mach number was less than unity. The contour of the averaged OH radical mass fraction, integrated over the lateral direction, is also shown in Fig. 8c. The averaged OH mass fraction was high in the shear flow region between the main airflow and the cavity recirculating flow, indicating that ethylene burned well. The Injector 1 fuel flow was cold until it reached the upstream edge of the cavity.

In contrast, the temperature of the Injector 2 fuel flow started to rise slightly downstream of the Injector 2 hole. The averaged OH mass fraction also rose downstream of Injector 2, indicating that the Injector 2 fuel burned. The Injector 2 fuel combustion was likely supported by radicals and increased gas temperature produced by the combustion of the Injector 1 fuel. Since the pressure in the cavity section rose due to the ethylene combustion, an oblique shock wave was generated in the main airflow near the cavity upstream edge. The main airflow converged in the cross-section toward the center axis of the combustor. After that, the main airflow diverged when the reflected shock wave from the combustor cross-section center was incident on the shear flow. The recirculating flow penetrated upstream beyond the cavity upstream edge when the cavity's pressure rose, causing the boundary layer separation.

3.3 Observation of ethylene flame in the combustor

Figure 9 shows the flame structure inside the combustor under each fuel injection condition. The figure is a single frame image from the video recorded in the KWT combustion tests at 30 fps. The orange arrows in Fig. 9 indicate the positions of Injectors 1 and 2, and the length of the arrow represents the fuel mass flow rate supplied from each injector. The cavity flame holder was type β, which was 18.2 mm deep. Injector 1 was type b, with two 3.4 mm holes and 25.4 mm spacing. Injector 2 was type B, with one 3.6 mm hole. The pale blue area in each figure was due to self-emission by the ethylene flame. The red emission was believed to be due to a deposit adhering to the observation window glass being heated. The source of the deposit was considered to be oil mist, which came from the air compressor to accumulate high-pressure air.

The streamwise distributions of the combustor wall pressure for all the cases shown in Fig. 9, normalized by the total pressure of the facility test flow, are also shown in Fig. 10. The X coordinate origin is at the entrance of the diverging-area combustor. The solid red squares and green circles show the wall pressure on the top and bottom walls with fuel supply, respectively. The open symbols show the wall pressures without a fuel supply for reference. The combustor flow-path shape with the fuel injector location is also shown at the bottom of each figure for reference. Note that the discontinuity in the pressure distribution around $X = -150$ mm and some bumps at $X = 50$–120 mm were due to the incidence of the compression waves or weak shock waves produced

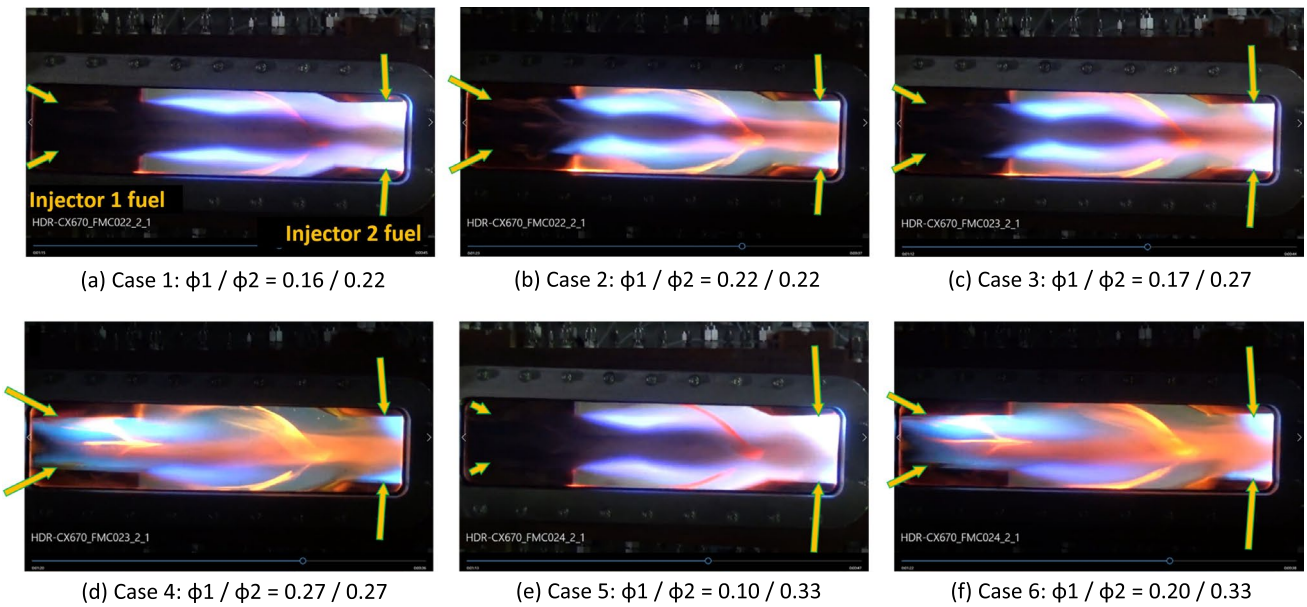

(a) Case 1: ϕ1 / ϕ2 = 0.16 / 0.22 (b) Case 2: ϕ1 / ϕ2 = 0.22 / 0.22 (c) Case 3: ϕ1 / ϕ2 = 0.17 / 0.27

(d) Case 4: ϕ1 / ϕ2 = 0.27 / 0.27 (e) Case 5: ϕ1 / ϕ2 = 0.10 / 0.33 (f) Case 6: ϕ1 / ϕ2 = 0.20 / 0.33

Fig. 9 Single frame images of ethylene flame in combustor model for each fuel injection condition: cavity flame holder of type β, Injector 1 of type b, Injector 2 of type B; ϕ1 and ϕ2 denote equivalence ratios of ethylene supplied from Injectors 1 and 2, respectively

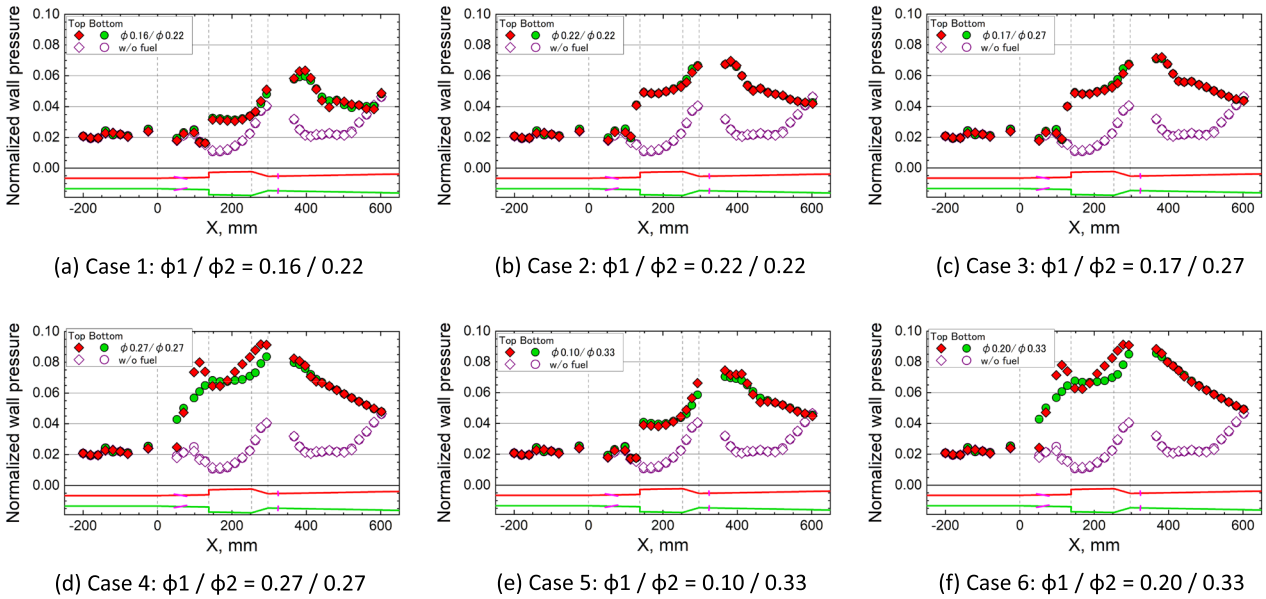

Fig. 10 Streamwise distributions of wall pressure normalized by test flow total pressure for each fuel injection condition; cavity flame holder of type β, Injector 1 of type b, Injector 2 of type B

by the incomplete wave cancelation of the facility nozzle at the present test flow condition. Although not shown, similar discontinuities and bumps appeared in the CFD-predicted wall pressure distribution. Small changes in Mach number due to these waves can be seen in the isolator section of the Mach number contours shown in Fig. 8b.

In all the pictures in Fig. 9 and the wall pressure distributions in Fig. 10, ethylene fuel supplied from Injectors 1 and 2 burned well. The more ethylene fuel supplied, the stronger the luminosity of the ethylene flame became, and the higher the combustor pressure rose. With the injection conditions of cases 1, 2, 3, and 5, where the total equivalence ratio was 0.44 or lower, the ethylene flame was almost symmetrical in the combustor height direction, and the pressure distributions on the top and bottom walls agreed well. In contrast, in cases 4 and 6, where the total equivalence ratio was 0.54, the flame luminosity of ethylene fuel supplied from Injector 1 was noticeably stronger. It spread more widely near the top wall than the bottom wall. The flame around the Injector 2 hole on the top wall penetrated high into the main airflow, while the flame on the bottom wall side was stretched in the main airflow direction. In Fig. 10d, f, there was a discrepancy between the pressure distribution on the top and bottom walls. At $X = 52$ mm, just upstream of Injector 1, the pressure on the bottom wall rose while that on the top wall remained as low as that without fuel injection. In contrast, the pressure on the top wall was higher than on the bottom wall at $X = 98$ mm, 113 mm, and 128 mm. Those were located between Injector 1 and the cavity upstream edge. Although the top wall pressure became almost the same or only slightly lower than the bottom one at $X = 148$ mm and 168 mm in the cavity, the top wall pressure became higher than the bottom one again in the X range from 208 to 293 mm, which was on the downstream half of the cavity bottom and the cavity aft-ramp. The results showed that the combustor flow became significantly asymmetric with the fuel supply conditions in cases 4 and 6. In case 1, where the total equivalence ratio was the lowest, and case 5, where the equivalence ratio of Injector 1 was only 0.1 while the total equivalence ratio was the same as in cases 2 and 3, the flame was formed from the upstream edge of the cavity and was stretched along the shear layer between the main airflow and the recirculating flow in the cavity. In cases 2 and 3, where the total equivalence ratio was 0.44, a part of the recirculating flow region in the cavity penetrated upstream beyond the cavity upstream edge because more fuel was supplied and the pressure in the cavity rose. As a result, the pale emission region spread upstream. The difference can be confirmed by the wall pressure distribution shown in Fig. 10. The pressure at $X = 128$ mm, just upstream of the cavity upstream edge, became much higher than that without fuel injection in cases 2 and 3, while it remained low in cases 1 and 5. In cases 4 and 6, where the total equivalence ratio was the highest, the recirculation region reached further upstream, and the combustor flow became fully asymmetric.

As mentioned in "Introduction" section, transition to the asymmetric combustor flow was newly found in the present combustion tests. An asymmetric flow is more difficult for CFD to simulate accurately than a symmetric flow, so it is unsuitable for CFD validation. The upper limit of the total

equivalence ratio in our study, for which the symmetric combustor flow can be maintained, was 0.44.

Based on the discussion above, we decided to evaluate the candidate combustor configurations by the combustion test results with the fuel injection cases 2 and 3, where the total equivalence ratio was 0.44. However, the split ratio between Injector 1 and Injector 2 was different. The upper limit equivalence ratio of 0.44 was 12% lower than the target value of 0.5, which had been set from the CFD study assuming the symmetry of the combustor flows.

The root cause of the considerably asymmetric combustor flow was believed to be that there was no particular anchor point to restrain the upstream propagation of the separation point when the combustor pressure rose, and the recirculating flow in the cavity penetrated upstream beyond the cavity upstream edge. The details of the discussion are described in the "Appendix".

3.4 Influence of the cavity depth on combustion characteristics

Figure 11 compares the wall pressure distributions with the different cavity depths: 25.7 mm, 18.2 mm, and 12.85 mm, referred to as the types α, β, and γ in Table 1. The aperture length was 159 mm for all three cavities; Injector 1 was type *b,* and Injector 2 was type *B*. The left and right figures show the results with the fuel supply condition of cases 2 and 3, respectively. The wall pressure distributions along the center line of the top wall and those of the bottom wall are shown. In addition, the results with and without fuel supply are shown by solid symbols and open symbols, respectively. The upper half of the combustor flow-path shapes and the injector locations are also shown in Fig. 11.

With fuel supply, the pressure rise due to ethylene fuel combustion started slightly upstream of the cavity upstream edge because, as shown in Fig. 9b, c, part of the recirculating flow region in the cavity penetrated upstream beyond the edge. The pressure continued to rise gradually toward the cavity aft-ramp end, and then, it reached its peak value around Injector 2. Downstream of Injector 2, the pressure dropped monotonically in the downstream direction as the cross-sectional area of the combustor duct increased. Without a fuel supply, the pressure dropped at the cavity upstream edge due to the sudden expansion of the flow path in the cavity section. The pressure rose rapidly in the cavity toward its aft-ramp, reaching its peak value near the downstream edge of the cavity aft-ramp. This peak is due to a shock wave produced by the impingement of the shear layer between the main airflow and the cavity recirculating flow on the cavity aft-ramp. Downstream of Injector 2, the pressure dropped due to the flow-path expansion. The pressure recovery near the exit of the combustor duct was due to the boundary layer separation against high back pressure.

The pressure in the cavity section tended to be higher with the shallower cavity, but only slightly. This trend is clearly seen in the wall pressure distribution without fuel supply. The pressure difference between the type α cavity and type γ one was larger without fuel supply than with it. The main reason for the slightly higher pressure with the shallower cavity was less expansion of the main airflow in the cavity section because the change of the flow-path cross-sectional area was smaller with a shallower cavity than a deeper one. With fuel supply, the pressure in the cavity flame holder rose due to combustion, and the recirculation region tended to expand and push the shear layer toward the center axis of the combustor. Consequently, the influence of the sudden expansion of the flow-path cross-sectional area on the combustor flow became weaker with fuel supply than without it. The result suggested that the combustion efficiency with the type γ cavity would remain almost the same

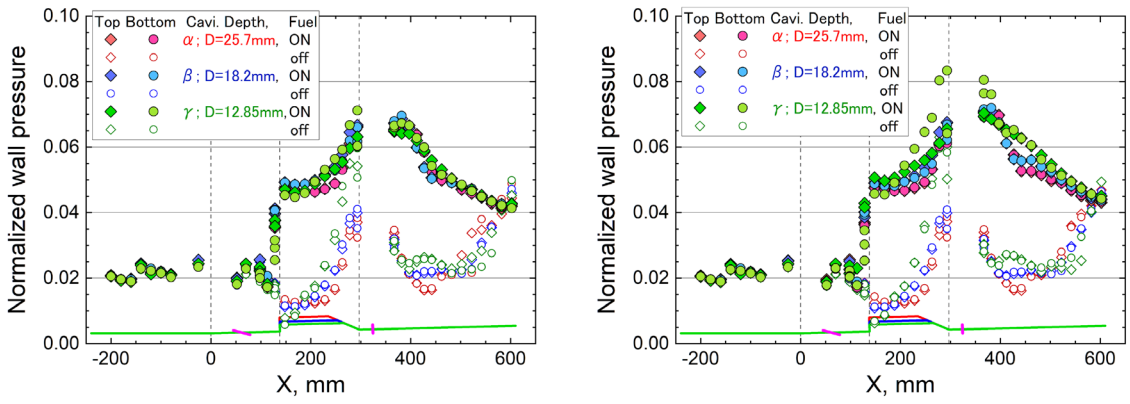

(a) Case 2; $\phi 1/\phi 2 = 0.22 / 0.22$

(b) Case 3; $\phi 1/\phi 2 = 0.17 / 0.27$

Fig. 11 Influence of cavity depth on wall pressure distributions: Injector 1 of type *b*; Injector 2 of type *B*

as that with the type α one. It is noted that CFD predicted almost the same structure of the combustor flow for the three cavities, except those in the cavity flame holder. The predicted streamwise distribution of the wall pressure and the mixing and combustion efficiencies were almost the same for the three cavities [10]. The interesting point of the CFD results was that the flow in the cavity recirculated mainly in a plane parallel to the center plane of symmetry in the lateral direction for the type α and type β cavities and that the flow recirculated mainly in a plane parallel to the center plane of symmetry in the vertical direction for the type γ. The type α cavity was 25.7 mm deep, almost half the combustor width. Thus, the size of the recirculating flow formed in the cavity was almost the same for the three cavities. However, it was difficult to determine how the recirculating flow was formed in each cavity in the tests. The pressure in the combustor was almost the same or slightly higher. Hence, the combustion efficiency of the type γ cavity was also likely to be the same or slightly higher than the other types. The CFD prediction seemed to agree with the combustion test results.

The combustion tests also showed that the wall pressure distribution on the top and bottom walls agreed well with the results shown in Fig. 11a, b, except those with the type γ cavity and the fuel supply condition of case 3, in which there was a discrepancy between the wall pressure distribution on the top wall and that on the bottom wall, so that the combustor flow was asymmetric. This suggests that the margin for maintaining the symmetry of the combustor flow was smaller with the type γ cavity than with the other two cavities.

We also evaluated the self-ignition capability of the ethylene fuel without the pilot hydrogen injection, considering recovery from an ignition failure using the pilot hydrogen or the flame-holding failure of ethylene. The results showed that the self-ignition capability of the type β cavity was the best of the three. With the deep type α cavity, the pressure and temperature drop due to the main airflow expansion in the cavity section was the largest among these three cavities. Hence, the reaction rate to initiate ethylene ignition was low. In contrast, a recirculating flow would likely not form in the shallow type γ cavity unless combustion occurred so that the residence time of the fuel–air mixture in the cavity was insufficient to initiate ethylene ignition.

Based on the above discussion, we selected the type β cavity for the RD1 combustor, with a depth of 18.2 mm.

3.5 Influence of the Injector 2 configuration on combustion characteristics

Figure 12 compares the wall pressure distributions measured with the different configurations of Injector 2. The cavity was type β, and Injector 1 was type b. For Injector 2, the number of injection holes had an observed effect on the wall pressure distribution. The pressure in the cavity section with the two-hole injectors was higher than that with a single hole. However, with fuel supply in case 3, there was a difference between the wall pressure distribution on the top wall and that on the bottom wall, and the combustor flow was asymmetric with the two-hole injectors. Therefore, the candidates for Injector 2 were narrowed down to single-hole injectors. However, the influence of the hole diameter on the combustion characteristics was not clear from the wall pressure distribution. Considering the RD1 flight experiment, the ethylene tank pressure first dropped rapidly since the ethylene was supplied in a blowdown manner. Second, the combustion test was conducted in the descent phase of the FEV flight, and the flight dynamic pressure rose from 25 to 100 kPa within several seconds of the flight test, so a high mass flow rate of ethylene would be required near the end of the test. Therefore, the injection hole with a large diameter

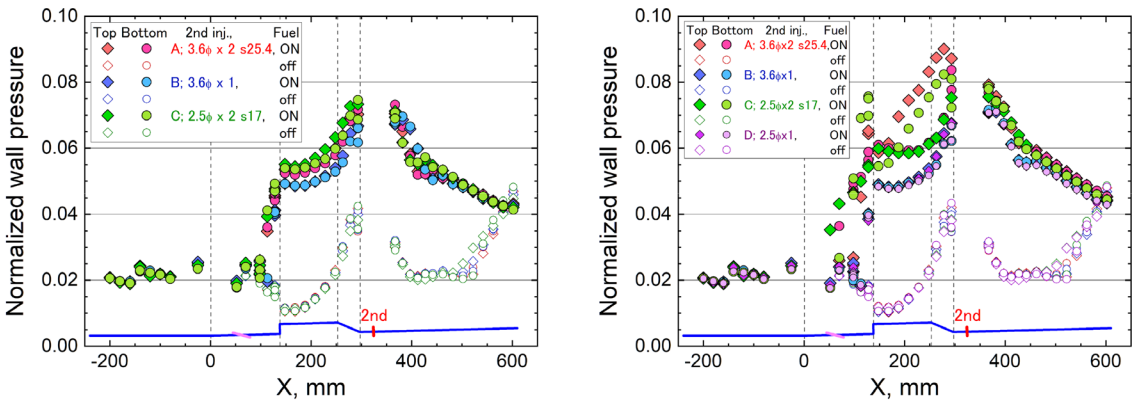

(a) Case 2; $\phi 1/\phi 2 = 0.22 / 0.22$

(b) Case 3; $\phi 1/\phi 2 = 0.17 / 0.27$

Fig. 12 Influence of the Injector 2 configuration on wall pressure distributions: cavity flame holder of type β, Injector 1 of type b

was preferred. Based on this, we adopted the type *B* Injector 2 with one 3.6 mm hole.

3.6 Influence of the Injector 1 configuration on combustion characteristics

Figure 13 compares the wall pressure distributions measured with the different configurations of Injector 1. The cavity was type β, and Injector 2 was type *B*. Although the result is not shown here, the pressure rise due to combustion in the cavity region was smaller with the single-hole injector than with the two-hole injector, especially with low equivalence ratios. Therefore, the candidates for Injector 1 were narrowed down to the two-hole injectors. In comparing the two-hole injectors tested here, we found that the influence of the Injector 1 configuration on the wall pressure distribution was small. For hole spacing, the wall pressure distributions with types *b* and *c* were almost the same, so the influence of the hole spacing was small. Injector hole diameters with the same spacing were compared. The pressure with 3.4 mm holes of type *c* was slightly higher than that with 2.4 mm holes of type *d*. There was a weak tendency for larger hole diameters to cause higher cavity pressures, but the difference was small. Considering the requirement to supply ethylene fuel at a large mass flow rate in the latter half of the RD1 flight experiment, an injection hole with a large diameter is best, so we adopted the type *b* configuration for Injector 1, which is the two-hole type with 3.4 mm holes 25.4 mm apart.

3.7 Influence of fuel supply ratio between Injectors 1 and 2 on combustion characteristics

In Figs. 11, 12 and 13, the wall pressure downstream of Injector 2 was always slightly higher for case 3 than case 2 because more ethylene fuel was supplied from Injector 2 than Injector 1, and the combustion heat released by the ethylene from Injector 2 was larger with case 3. This was seen in the wall pressure distributions with the type γ cavity in Fig. 11b and with the Injector 2 s of types *A* and *C* in Fig. 12b, which reflected the results of case 3. A discrepancy between the wall pressure distribution on the top and bottom walls causes an asymmetric combustor flow. The results suggested that the fuel supply in case 2 had a larger margin in maintaining a symmetric combustor flow than in case 3. Consequently, the fuel supply condition of case 2, with the split ratio between Injector 1 and Injector 2 of one-to-one, was chosen for the RD1 combustor.

3.8 Selection of the configuration and the fuel supply condition for the RD1 combustor

The combustor configuration and the fuel supply condition for the RD1 combustor model, those proposed by the present study, are summarized as follows. The selected configuration is the same as that shown in Fig. 2.

(1) The cavity depth of type β was 18.2 mm;
(2) The Injector 1 configuration was type *b*, with two 3.4 mm holes and 25.4 mm spacing:
(3) The Injector 2 configuration was type *B*, with one 3.6 mm hole; and
(4) The total fuel equivalence ratio, with which the symmetric combustor flow can be maintained, was 0.44. The split ratio of the fuel supply between Injectors 1 and 2 was selected to be one-to-one.

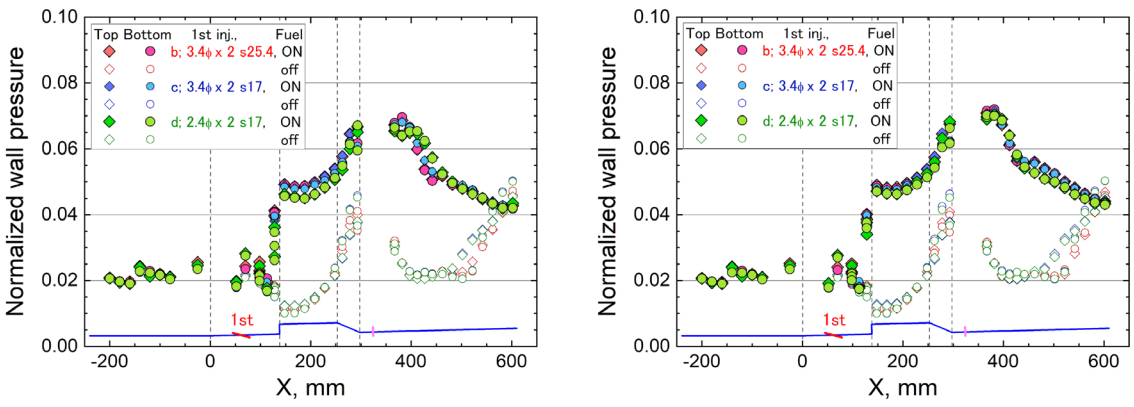

(a) Case 2; $\phi 1/\phi 2 = 0.22 / 0.22$

(b) Case 3; $\phi 1/\phi 2 = 0.17 / 0.27$

Fig. 13 Influence of the Injector 1 configuration on wall pressure distributions: cavity flame holder of type β, Injector 2 of type *B*

3.9 Demonstration of ethylene ignition method by pilot hydrogen injection

It was confirmed that ethylene fuel was ignited by the pilot hydrogen injection in this test in the KWT. In the first step of the demonstration, the pilot hydrogen was supplied steadily to the combustor model using the hydrogen gas supply system of the KWT. The hydrogen supply pressure was regulated to 2.2 MPa for the nominal test flow with a total pressure of 2 MPa and a total temperature of 1700 K. To control the hydrogen mass flow rate, an orifice with a hole diameter of 2 mm was installed in the supply line. With this setup, the equivalence ratio of the pilot hydrogen was 0.21. It was found that the key to igniting ethylene fuel is to provide time to overlap the pilot hydrogen supply and the ethylene fuel supply. The overlap time of the hydrogen and ethylene supplies was set for 0.3 s. In the direct-connect combustor test case, the pressure at the combustor exit was lower than the ambient atmospheric pressure before the pilot hydrogen supply started. This resulted in boundary layer separation near the combustor exit. In an actual flight test, the ambient pressure is usually lower than the combustor exit pressure, so boundary layer separation will not occur. Therefore, if the first ignition occurred within the separation region near the combustor exit in the present ground test and the flame traveled upstream to the cavity flame holder region, starting combustion there, the feasibility of the ethylene ignition method using pilot hydrogen could not be adequately evaluated. Figure 14 shows the time variation of the pressure distribution in the combustor model at intervals of 0.05 s before and after the self-ignition of pilot hydrogen occurred. Only the pressure distributions on the top wall are shown in Fig. 14 because those on the bottom wall were substantially the same. Pilot hydrogen was supplied only from Injector 1, located upstream of the cavity flame holder. Before the pilot hydrogen supply started, boundary layer separation occurred near the combustor exit. However, Fig. 14 clearly shows that the pressure began to rise mainly around the cavity aft-ramp and in the cavity at a time between $t = 13.047$ s and 13.097 s. In contrast, the pressure around the separation point near the combustor exit remained low. If the ignition of pilot hydrogen occurred first in the separation region near the combustor exit and the flame traveled upstream, starting combustion there, the high-pressure region should have traveled upstream from near the exit to the cavity region in Fig. 14. However, no such signs are seen in Fig. 14. Thus, we concluded that the self-ignition of pilot hydrogen occurred around the cavity aft-ramp or in the recirculating flow inside the cavity. Before the pilot hydrogen supply started, a high-pressure peak appeared around the cavity aft-ramp due to strong impingement of the shear flow between the main airflow and the recirculating flow in the cavity on the cavity aft-ramp, forming a shock wave. In addition, Fig. 7 shows that the wall temperature was high at $X = 293$ mm, located on the cavity aft-ramp. Therefore, the area around the cavity aft-ramp was where pressure and temperature tended to be higher and flow velocity slower. Therefore, it was suitable for the self-ignition of pilot hydrogen.

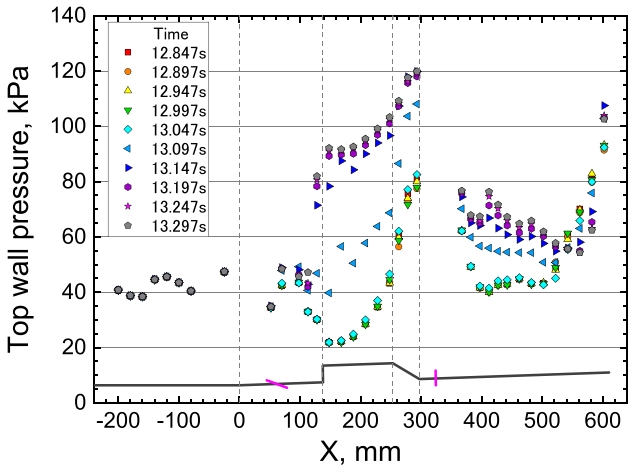

Fig. 14 Time variation of the wall pressure distribution on the top wall of the combustor model during the ignition process of pilot hydrogen; the total pressure was 2 MPa, and the total temperature was 1700 K; cavity flame holder of type β, Injector 1 of type b, Injector 2 of type B

Assuming the application of the present ignition method to the combustion test of a full flow-path combustor model, which includes an inlet and a downstream extension duct, in the RJTF, the present method was further demonstrated at the test flow condition with the total pressure of 1.5 MPa and the total temperature of 1570 K. Then, it was confirmed that ethylene could be successfully ignited at low-pressure and low-temperature flow conditions. Although the results are not shown here, it was also confirmed that pilot hydrogen self-ignited near the cavity aft-ramp or in the recirculating flow inside the cavity under these conditions. The time variation of the wall pressure distribution in the combustor model was quite similar to that shown in Fig. 14.

Next, the ignition method of supplying the pilot hydrogen stored in a 1 L run tank in a blowdown manner was also demonstrated, assuming the application of the present method to the actual RD1 FEV. Once the pilot hydrogen starts to be supplied, the pressure in the hydrogen tank drops rapidly. It is necessary to set the initial filling pressure higher than for the steady supply using the facility hydrogen supply system of the KWT. For this setup, the orifice was replaced by one with a hole diameter of 1.4 mm. The combustion test confirmed that the ethylene could be ignited with a feasible initial filling pressure of the hydrogen tank; that is, 4.1 MPa for the test flow with a total pressure of 1.5 MPa and a total temperature of 1570 K.

4 Conclusions

The direct-connect combustion tests of the supersonic combustor model for the RD1 flight experiment vehicle were conducted using the vitiation-air-heater-type supersonic wind tunnel at JAXA Kakuda Space Center to investigate the influence of the depth of the cavity flame holder and the configuration of the injection holes (i.e., the number and diameter of the injection holes for Injectors 1 and 2) on the combustion characteristics. The final combustor flow-path design was based on the test results. The feasibility of igniting ethylene fuel using pilot hydrogen injection was also demonstrated for the RD1 flight experiment. The following results were obtained.

(1) The combustion test results showed that symmetry of the combustor flow was maintained when the total equivalence ratio of ethylene fuel was low, but the combustor flow tended to become asymmetric in the combustor height direction as the fuel equivalence ratio increased and the combustor pressure became high while the supersonic combustion mode operation was still maintained. Since the asymmetric combustor flow is unsuitable for CFD validation, the second requirement for the combustor flow-path design became a symmetric combustor flow in the supersonic combustion mode.
(2) The upper limit of the total equivalence ratio, with which the symmetric combustor flow could be maintained, was 0.44 under the test conditions. The split ratio of Injector 1 to Injector 2 was selected to be one-to-one for the same reason.
(3) The depth of the cavity flame holder had little influence on the wall pressure distribution in the combustor, as CFD had predicted. The 18.2 mm-deep cavity was selected because it was best for ethylene self-ignition.
(4) The number of injection holes in Injector 2 affected the wall pressure distribution in the combustor. The single-hole injector with the 3.6 mm hole was selected because it maintained a symmetric combustor flow better than the two-hole injector.
(5) The influence of the Injector 1 configuration on the wall pressure distribution was not as large as that of Injector 2. The two-hole injector with the 3.4 mm holes was selected since the two-hole injector with the large diameter showed an advantage in obtaining high pressure in the cavity with the wide range of the fuel equivalence ratio.
(6) The ethylene ignition method using the pilot hydrogen injection was demonstrated successfully. The key to the successful ignition was to provide sufficient time for the pilot hydrogen and ethylene fuel to be supplied simultaneously.

Appendix: Cause of the considerably asymmetric flow in the combustor

First, the influence of dimensional errors in the fabrication, assembly, and installation of the combustor model to the wind tunnel on the asymmetry of the combustor flow is discussed. The combustor model consisted of a top wall plate, a bottom wall plate, both side wall plates, and a flange at the upstream end. Aiming to reduce the manufacturing time because of the tight schedule of the research program, all these plates were bolted together to assemble the combustor with a 0.7 mm-thick GRAFOIL® sheet (NeoGraf Solutions) inserted between contact surfaces for sealing. The injector and cavity blocks were also attached to the top and bottom plates with bolts to allow for replacement. Consequently, the dimensional errors in the fabrication, assembly, and installation of the combustor model to the wind tunnel should have been present to some extent. However, the combustor flow with cases 1, 2, 3, and 5 was reasonably symmetric, as shown in Figs. 9 and 10. Therefore, it was reasonable to conclude that the influence of the dimensional errors was not a root cause for the considerably asymmetric combustor flow.

Second, the possible influence of uneven fuel supply from Injectors 1 and 2 on the top and bottom walls is discussed in causing the considerably asymmetric combustor flow. As mentioned in the "Fuel supply system" section, the facility fuel supply system and the injectors on the combustor model were acoustically isolated by the orifices in the fuel supply line. Figure 7 also showed that the pressure histories of the fuel manifold on the top and bottom walls agreed well for each injector, suggesting that the fuel supply from the top and bottom walls seemed to be even. In addition, according to the evaluation of the ratio of the pressure in the combustor near the injector hole to the fuel manifold pressure, the fuel flow choked at the injection hole of Injectors 1 and 2 in all the combustion tests, except the case for type *A* Injector 2, which had the largest injection hole area. As long as the choke condition was maintained at the injection hole, the interaction of the fuel flow supplied from the injection holes on the top and bottom walls would hardly occur. From the discussion above, the uneven fuel supply from the top and bottom walls was unlikely to occur in the present combustion tests.

The difference between the estimated normal force imposed on the top and bottom walls is shown in Fig. 15 against the ratios of the wall pressure near the injection hole to the fuel manifold pressure. The normal force on each wall was estimated by surface-area weighted integration of the wall pressures measured from $X = 98$ mm to $X = 293$ mm.

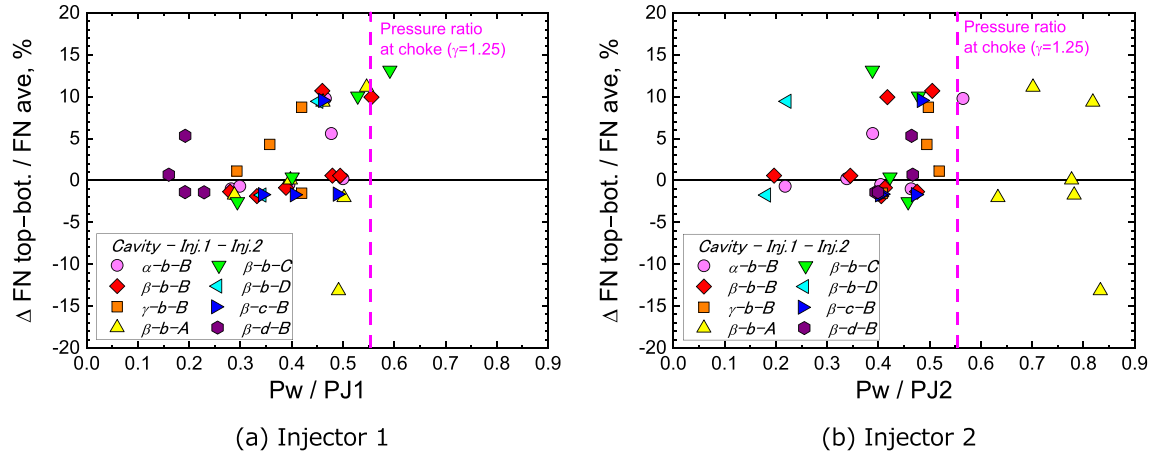

Fig. 15 Relation between the ratio of wall pressure near the injector hole and the fuel manifold pressure and the difference between the normal force imposed on the top and bottom walls, normalized by the averaged normal force

The positive value means that the normal force on the top wall was larger than that on the bottom. The difference of the normal forces shown in Fig. 15 was normalized by those averaged forces. The wall pressure near the injection hole took the higher value of the pressures measured at the two pressure ports adjacent to each injection hole. The pressure ratio for the choke condition, calculated under the assumption that the specific heat ratio of ethylene is constant at 1.25, is also shown in Fig. 15. As mentioned above, the measured pressure ratio was lower than the theoretical value for the choke condition, except for Injector 2 of type *A*, which has the largest hole area among the candidate configurations tested in the present study. The most important finding from Fig. 15 was that the large difference of the normal force due to the considerably asymmetric combustor flow appeared no matter if the fuel flow choked at the injection hole.

Next, the normalized difference of the normal force is shown in Fig. 16 against the averaged value of the normal force on the top and bottom walls. Figure 16 clearly shows that the larger the average normal force was, the larger the difference of the normal force between the top and bottom walls was. In other words, the higher the combustor pressure was, the more asymmetric the combustor flow became. When the combustor pressure was low, the recirculating flow in the cavity flame holder remained in the cavity. The cavity upstream edge likely served as an anchor point that suppressed the upstream penetration of the cavity recirculating flow due to increased combustor pressure. However, once the recirculating flow penetrates upstream beyond the upstream end of the cavity, there is no particular anchor point, such as a backward-facing step, on the upstream side to restrain the upstream propagation of the separation point so that the separation point location is likely to become sensitive to the change in the

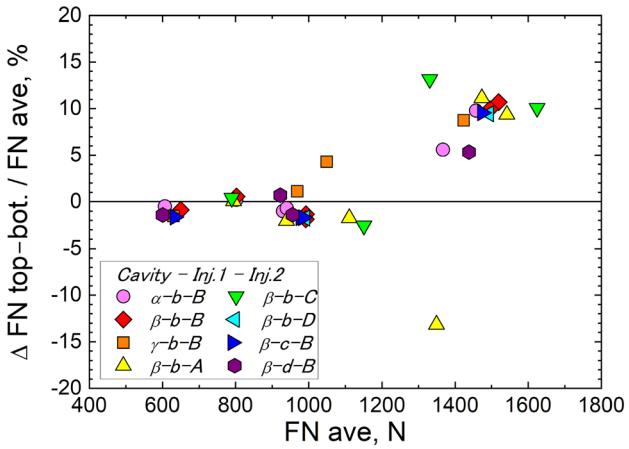

Fig. 16 Relation between the averaged normal force and the difference of the normal force imposed on the top and bottom walls, normalized by the averaged normal force

downstream pressure or the local deflection of the combustor flow around the separation region. From the discussion above, the root cause for the considerably asymmetric combustor flow was considered because there is no particular anchor point to restrain the upstream propagation of the separation point when the combustor pressure rises, and the recirculating flow in the cavity penetrates upstream beyond the cavity upstream edge.

Acknowledgements This work was supported by the Innovative Science and Technology Initiative for Security Grant Number JPJ004596, ATLA, Japan.

Data availability Not available.

Declarations

Conflict of interest The authors declare that they have no conflict of interest.

References

1. Yatsuyanagi, N., Chinzei, N., Mitani, T., Wakamatsu, Y., Masuya, G., Iwagami, S., Endo, M., Hanus, G.: Ramjet Engine Test Facility (RJTF) in NAL-KRC, Japan. AIAA Paper 1998-1511 (1998)
2. Tomioka, S., Hiraiwa, T., Kobayashi, K., Izumikawa, M., Kishida, T., Yamasaki, H.: Vitiation effects on scramjet engine performance in Mach 6 flight conditions. J. Propul. Power **23**, 789–796 (2007). https://doi.org/10.2514/1.28149
3. Pellett, G.L., Bruno, C., Chinitz, W.: Review of air vitiation effects on scramjet ignition and flameholding combustion processes. AIAA Paper 2002-3880 (2002)
4. Rockwell, R.D., Jr., Goyne, C.P., Haw, W., Krauss, R.H., McDaniel, J.C., Trefny, C.J.: Experimental study of test-medium vitiation effects on dual-mode scramjet performance. J. Propul. Power **27**, 1135–1142 (2011). https://doi.org/10.2514/1.B34180
5. Tatman, B.J., Rockwell, R.D., Goyne, C.P., McDaniel, J.C., Donohue, J.M.: Experimental study of vitiation effects on flameholding in a cavity flameholder. J. Propul. Power **29**, 417–423 (2011). https://doi.org/10.2514/1.B34687
6. Tani, K., Onodera, T., Kato, K., Takegoshi, M.: Flight experiment for the validation of new methodology to compensate the wind tunnel contamination problem. 32nd ISTS, Fukui, Japan, 2019-m-11 (2019)
7. Nagata, Y., Yokoi, S., Aoki, R., Kouchi, T., Yanase, S.: LES analysis of transverse jet mixing in supersonic free-stream turbulence. AIAA Paper 2020-1335 (2020)
8. Kodera, K., Takahashi, M., Kobayashi, K., Tomioka, S.: CFD Prediction of scramjet combustor performance for flight experiment, 3A02. In: Proceedings of the 61st Japanese Conference on Propulsion and Power (2022) **(in Japanese)**
9. Takahashi, M., Tomioka, S., Kodera, M., Kobayashi, K., Hasegawa, S., Shimizu, T., Aono, J., Munakata, T.: Numerical study on combustor flow-path design for a scramjet flight experiment. Trans. Jpn. Soc. Aeronaut. Space Sci. Aerosp. Tech. Jpn. **19**, 415–423 (2021). https://doi.org/10.2322/tastj.19.415
10. Takahashi, M., Tomioka, S.: Flow-path design of a combustor model for a supersonic-combustion flight experiment. In: 51st Japanese Fluid Dynamics Conference/37th Aerospace Numerical Simulation Symposium, Waseda, Tokyo, Japan, 1C14 (2019) **(in Japanese)**
11. Ogawa, S., Choi, B., Takita, K., Masuya, G.: Fuel mixing enhancement by pre-combustion shock wave. ISABE Paper 2001-1188 (2001)
12. Tomioka, S., Kouchi, T., Masumoto, R., Izumikawa, M., Matsuo, A.: Supersonic combustion with supersonic injection through diamond-shaped orifices. J. Propul. Power **27**, 1196–1203 (2011)
13. Jackson, K.R., Gruber, M.R.: HIFiRE Flight 2—a program overview. In: 51st AIAA Aerospace Sciences Meeting Including the New Horizons Forum and Aerospace Exposition Grapevine, Texas, U.S.A, AIAA Paper 2013-0695 (2013)
14. Kitamura, K., Fujimoto, K., Kuzuu, K., Shima, E., Wang, Z.J.: Validation of arbitrary unstructured CFD code for aerodynamic analyses. Trans. Jpn. Soc. Aeronaut. Space Sci. **53**, 311–319 (2011)
15. Kitamura, K., Shima, E.: Towards shock-stable and accurate hypersonic heating computations: a new pressure flux for AUSM-family schemes. J. Comput. Phys. **245**, 62–83 (2013)
16. Menter, F.R.: Zonal two equation k-omega turbulence models for aerodynamic flows. AIAA Paper 93-2906 (1993)
17. Kobayashi, K., Tomioka, S., Takahashi, M., Kodera, M.: Reaction mechanism reduction for ethylene-fueled supersonic combustion CFD. CEAS Space J. (2023). https://doi.org/10.1007/s12567-023-00484-1